RSC Advances

ROYAL SOCIETY OF CHEMISTRY

www.rsc.org/advances

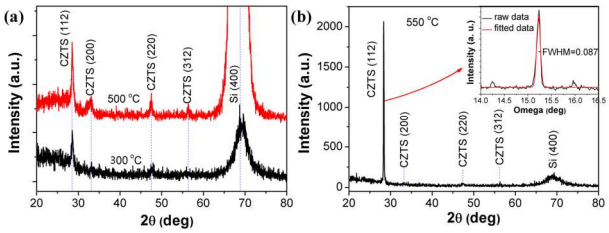

CZTS fibers with strong (112) orientational crystallization are fabricated on Si substrates.

Electrospun Cu_2ZnSnS_4 microfibers with strong (112) preferred orientation: fabrication and characterization

Chunhong Mu,[1] Yuanqiang Song,[1] Aifang Liu,[1] Xiaoning Wang,[1] Jiarui Hu,[1] Hong Ji,[1] Hongping Zhang[2]*

[1]School of Energy Science and Engineering, University of Electronic Science and Technology of China, Chengdu 610054, People's Republic of China

[2]School of materials Science and Engineering, Southwest University of Science and Technology, Mianyang 621010, People's Republic of China

[*]E-Mail: yuanqiangsong@uestc.edu.cn

Abstract

In this work, Cu_2ZnSnS_4 (CZTS) microfibers were fabricated using a non-vacuum method of electrospinning following vulcanization process. CZTS fibers were obtained *via* vulcanization the electrospun precursor fibers at 500 ℃ (CZTS-500), 550 ℃ (CZTS-550), and 600 ℃ (CZTS-600), respectively, in sulfur ambient. Samples were characterized by Scanning electron microscopy (SEM) equipped with Energy-dispersive spectroscopy (EDS), X-ray diffraction (XRD), XRD mapping scan, Raman spectrum and UV-vis absorption. Polycrystalline CZTS fibers with kesterite crystallization were formed in CZTS-500, while higher temperature vulcanization in CZTS-550 led to a strong preferential crystallization along CZTS [112] crystal direction around fiber surface, which is definitely confirmed by XRD mapping scan. More interestingly, the band gap value (E_g), which was 1.48 eV for

CZTS-500, reduced to 1.43 eV for CZTS-550. E_g reduction may be related with lattice distortion induced by stress or strain around fiber surface, and shall be beneficial for broadening optical absorption range thus increasing the efficiency of CZTS-based solar cells.

1. Introduction

The third generation solar cells based on new type of thin film semiconductors such as $CuIn_xGa_{1-x}Se_2$ (CIGS),[1] $CuInS_2$ (CIS),[2] Cu_2ZnSnS_4 (CZTS),[3] are one promising candidate for the low cost commercialized solar cell products. CIGS is one of the most successful thin-film photovoltaic materials, based on which the fabricated cells reach recently a power conversion efficiency of nearly 20%.[4,5] However, four rare elements composed of CIGS make a high-cost for CIGS-based cell production. On the other hand, the four elements composing of CZTS is natural abundant and environmental harmless, this makes CZST one of the most promising candidate for large-scale commercial applications.

As a p-type direct band gap semiconductor, CZTS with the crystal structure and optical properties similar to those of CIGS, is also an excellent absorbance for solar spectra (its band gap is about 1.5 eV and absorbance coefficient about 10^4 cm^{-1}). However, the low photoelectric conversion efficiency[6-8] of CZTS-based cells is yet one of the biggest obstacle limiting its commercial applications. The highest efficiencies reported to date were obtained from the cells using CZTS absorbed layer with large grain size and high film quality.[6,7] The grain size grows nearly to 2 μm in

$Cu_2ZnSn(S,Se)_4$ (CZTSSe) solar cells with a high efficiency beyond 11%.[9] The recently reported highest efficiency measured in CZTSSe solar cells can also be partially attributed to fine crystallization with large grain size.[10] However, these efficiencies in CZTS or CZTS based solar cells are far away from the efficiencies which can be comparable to CIGS.[11]

Previous studies have confirmed grain boundary (GB) as the attribution to high efficiency for CIGS solar cells.[12-16] With the aid of these GBs, where it presents an electric field in the vicinity of the GBs, minority carriers move much easier to the n-type CdS and ZnO layers leading to an enhanced minority carrier collection.[13] GBs in CZTS, however, would cause two contradictory effects on the efficiency. On one hand, higher positive surface potential has been found in the vicinity of the GBs in CZTS,[17] which can benefit the minority carriers collection as well as the efficiency. On the other hand, the GBs in CZTS would also create more defect levels in the energy gap of CZTS compared to CIGS.[18] These defects would be detrimental to the charge separation by promoting the recombination of excited electron and hole carriers and therefore reduce the solar cell's efficiency. All things considered, GBs would be one of the main factors limiting the efficiency of CZTS solar cell, according to recently experimental report of the limited efficiency of CZTS solar cells compared with CIGS. Based on this speculation, either effective passivation treatment of GBs or decreasing the GBs density would be needed to improve the efficiency.

Nanoarray *p-n* junctions has been adopted in silicon nanowire-based solar

cells,[19] for the purpose of efficiency enhancement.[20,21] The mechanism corresponding to the enhancement of photoelectric conversion efficiency in nano-structured solar cells is supposed to be (a) nano-structured cells' surface would trap much more light with a highly reduced reflectance, and (b) much higher specific surface area would be obtained in the nano-structured *p-n* junctions, for the utilization of photo absorption as well as photoelectric generation, leading to higher photoelectric conversion efficiency. This efficiency-enhancement method is readily applied to CZTS solar cells, provided that the technology for production of nano-structured CZTS can be developed. According to previously report, CuSe and $CuInSe_2$ nano-bundles have been successfully fabricated *via* a facile and promising solvothermal method.[22] CZTS nanorods have also been successfully synthesized, using anodized aluminums as the growth mask or template.[23-25] For the first time, CZTS fibers were fabricated by Hsu *et al* using electrospinning process.[26] As a low-cost, non vacuum and productive method widely used for production of nano-structured fibers, electrospinning should be acquired more attentions, focusing on fabrication and growth mechanism of CZTS nanofibers. In this report, single-phased CZTS microfibers are successfully synthesized *via* electrospinning following vulcanization approach. While well crystallized CZTS fibers in kesterite can be obtained by vulcanization at 500 ℃, higher vulcanization temperature at 550 ℃ lead to strong [112] preferential crystallization in kesterite [112] direction around CZTS fiber surface. Even more, the band gap (E_g) of CZTS fibers reduced from 1.48

eV to 1.43 eV coupling with [112] preferential orientation growth. The preferential growth as well as reduced E_g are beneficial for exploring high-efficiency CZTS-based solar cells.

2. Experimental details

$Cu(CH_3COO)_2$, $Zn(CH_3COO)_2$ and $SnCl_4$ are weighed and mixed according to the stoichiometry of Cu_2ZnSnS_4 compound, and then dissolve the mixture and certain amount of polyvinylpyrrolidone (PVP) into ethylene glycol monomethyl ether, stirring during the dissolving process to form transparent solution. The solution is pumped into a plastic syringe, then ejects out from a metal needle with 0.6 mm in diameter. The precursor fibers are collected on Si (100) substrates connected with the ground. The distance between the needle and the collector plane is kept as 5 centimeter, and a high voltage of 10 KV is applied between them.

Vulcanization is carried out in a tube furnace. The precursor microfibers on silicon substrates are firstly dried at 80 ℃ for 2h. In order to avoiding any possible carbon residue in the final products, the dried precursor fibers are annealed at 300℃ for 30 minutes at atmosphere before vulcanization. Vulcanization process is carried out at 500℃ (CZTS-500), 550℃ (CZTS-550), and 600℃ (CZTS-600), for 1h in sulfur ambient, respectively. During the vulcanization process Ar is used as the protective gas and carrier.

3. Characterization

The morphologies of the CZTS microfibers were characterized by SEM (JEOL

Ltd.). The compositions as well as the elemental ratio of each element was obtained by EDS equipped on SEM. Crystallographic information on CZTS crystals was obtained *via* XRD carried out on Bede D1 diffractometer operating in the Bragg configuration, using a monochromatized Cu Kα radiation (λ = 1.540596 Å). Raman spectra measurements were performed using a Renishaw in Via Raman spectroscope in atmosphere at room temperature. The 325 nm line was used as the excitation source, with spectral resolution 4 cm^{-1}. The power density was kept under 5 mW, which is low enough to avoid heating effects on samples. Optical absorption properties were characterized in the wavelength range of 400-1200 nm *via* a UV-vis spectrometer (UV3600, SHIMADZU). In order to eliminate the scattering noise induced by non-uniform fibers structure, the reflection mode was adopted in optical measurement using an integrating sphere accessory.

4. Results and discussion

4.1 Micro morphologies of CZTS fibers

Figure 1 (a), (b), (c), (d) and (f) show the morphologies of the electrospun precursor fibers, CZTS-300, CZTS-500, CZTS-550, and CZTS-600, respectively. Clearly can be seen that, all samples except CZTS-600 are obviously composed of micro-fibers with varied diameters. The diameter of CZTS fibers firstly decrease (as shown in figure 1(b)) and then increase with increasing annealing temperature (as shown in figure 1(c) and (d)). The precursor fibers as shown in figure 1(a) are straight without any branch, and the diameter distribution is almost uniform with an average

diameter of submicron. The diameter is highly reduced by annealing at 300 ℃ as shown in figure 1(b), but the fibers still remain straight. For sample CZTS-500 as shown in figure 1(c), the diameter increases with the combination and interconnection of adjacent fibers leading to a porous netlike morphology, which is also the case for CZTS-550 with larger diameter. However, higher annealing temperature would cause obvious surface cracking due to excessive contraction, as shown in the case of CZTS-600. The much detailed morphology of the CZTS-550 surface is shown in figure 1(e), from which many micro gibbosities can be seen. The gibbosities may be crystal grains formed by vulcanization.

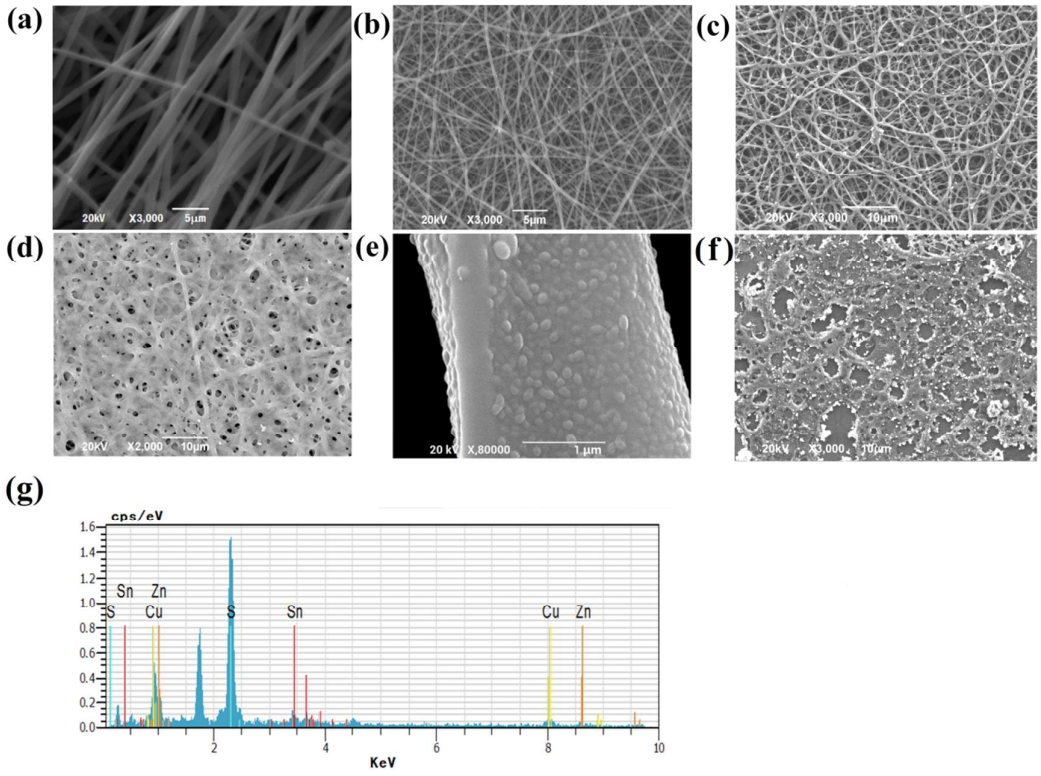

Fig. 1 Morphologies of (a) the as-electrospun precursor fibers, (b) samples annealed at 300 ℃ at atmosphere (named as CZTS-300), (c), (d) and (f) are samples vulcanized at 500 ℃, 550 ℃, and 600 ℃ (named as CZTS-500, CZTS-550, CZTS-600), respectively. (e) is the high-resolution SEM of one fiber of CZTS-550. The EDS spectrum of CZTS-550 is shown in (g).

Table 1 Elemental ratio of each element included in the CZTS-550 characterized by EDS.

Element	Weight ratio	Atomic ratio
S-32.06	31.97	53.30
Cu-63.54	27.26	22.93
Zn-65.38	14.72	12.03
Sn-118.6	26.05	11.74
Total	100.00	100.00

EDS has been obtained for elemental composition analysis. It shows almost the same composition and atomic ratio in CZTS-500 and CZTS-550, of which the data are provided in table 1 according to the EDS shown in fig. 1(e). It confirms the exclusively existence of four elements of Cu, Zn, Sn and S with the atomic ratio of 1.95: 1.025: 1: 4.54. There is a Cu/(Zn+Sn) ratio of 0.96 and a Zn/Sn ratio of 1.025, demonstrating a Cu-poor and Zn-rich composition, which would be beneficial to efficiency enhancement of CZTS based solar cells.[8,9]

4.2 Crystalline characterization

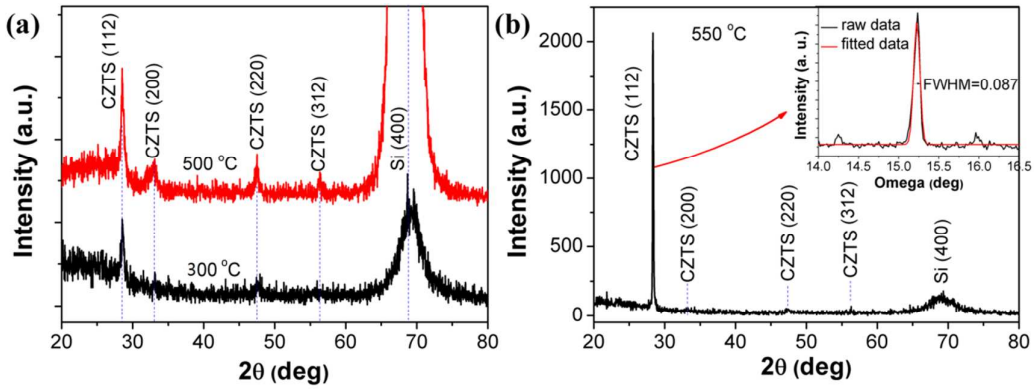

Fig. 2 XRD of (a) CZTS-300 and CZTS-500 as indicated in the figure, and (b) CZTS-550, in which the full width at half maximum (FWHM) of CZTS (112) is 0.087 as shown in the inset.

Figure 2 shows the X-ray diffraction (XRD) patterns of CZTS fibers annealed at

varied temperature. Obviously as shown in figure 2(a), annealing at 300 ℃ is enough to lead to partial crystallization with the emergence of CZTS (112) and (220) peak. For CZTS-500 obtained at higher vulcanization temperature, its XRD profile matched well with standard CZTS PDF card of kesterite crystal phase, confirming high crystallization and phase formation of CZTS fibers. For CZTS-550 with continued rising of vulcanization temperature, however, peak (112) was amazingly enhanced and other peaks are distinctively diminished. In fact, it seems only one diffractive peak emerges at the position of 2θ=28.35º, which is corresponding to the (112) peak of CZTS. The shape of the (112) peak is very narrow with a high intensity more than 2000. The results definitely indicate a preferential growth along [112] crystal direction in CZTS-550. The FWHM of (112) peak obtained from the rocking curve is 0.087 degree, as shown in the inset of figure 2 (b). Based on Scherrer-equation:

$$D = K\lambda/B\cos\theta \quad (1)$$

in which D is the grain size in nanometer unit, K is Scherrer constant (0.89), λ=0.154056 nm is the wave length of the X-ray, B is FWHM of the rocking curve, θ is the diffracting angle in degree, the calculated grain size is 93.13 nm.

Until now the kesterite crystalline CZTS microfibers are confirmed, and higher vulcanization temperature can lead to obvious preferential growth in (112) direction. Z. Q. Li *et al*[27] have successfully grown CZTS nanowires with polycrystal crystallization using CuSe nanowire bundles as self-sacrificial templates. Koichiro

Oishi *et al*[28] have recently reported an orientational growth of CZTS films in (200) direction with an increased growth temperature. In their experiments the CZTS films were grown on Si(100) by vacuum evaporation. However, the essential mechanism contributing to the good crystallization and strongly preferential growth of electrospun CZTS fibers may be different. Minimization of surface energy may contribute to (112) preferential growth in CZTS fiber system. It can be deduced that, CZTS (112) crystal surface is the easiest growth surface with the lowest free energy for the growth of electrospun CZTS microfibers, thus leading to a (112) preferential crystallization in the radial direction around the fiber surface.

In order to verify this hypothesis, XRD mapping scan around one CZTS fiber have been done according to the configuration shown in figure 3, and the corresponding scanning results are shown in figure 4.

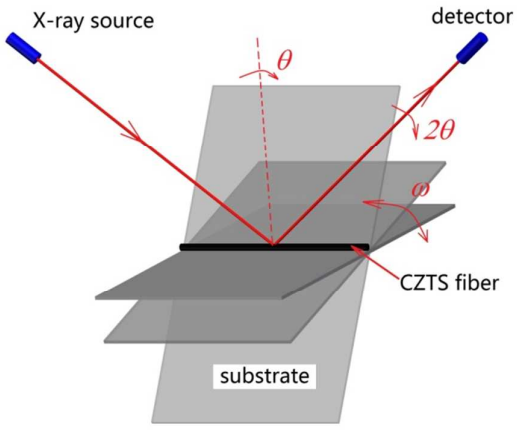

Fig. 3 Configuration of XRD mapping scan around one CZTS fiber. During the process, for each stepping rotation (ω) of the substrate, there is a θ-2θ scan.

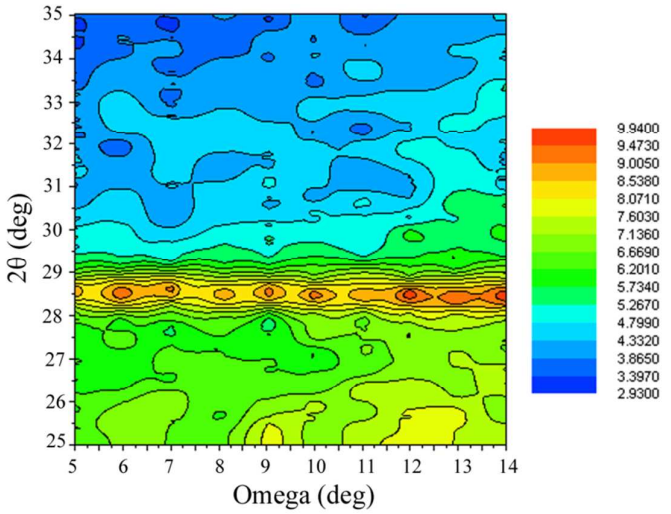

Fig. 4 XRD mapping scanned around one CZTS fiber according to the configuration shown in figure 3.

As clearly can be seen from figure 4 that, for each stepping rotation around one fiber, there emerges only one peak at 2θ = 28.35, which is just correspond to CZTS (112) diffraction peak. In other words, there is only one preferential crystallization along CZTS (112) out of the surface around the CZTS fiber. The fact can be reasonably explained by energy minimization principle in fiber-composed CZTS films. The specific surface area as well as surface energy for a crystal fiber with diameter in micro or even nano scale is very high, so the minimum energy plane is the easiest crystallization and growth direction. In CZTS system with a kesterite structure, the thermodynamic preferable growth direction will along (112) orientation, which is the close-packed plane in CZTS system. Here in CZTS fibers in micro or nano scale, the energetic driving force would be much higher due to the high surface energy. In fact, several groups have reported the preferential crystallization effect along (112) plane in CZTS films.[28,29]

4.3 Raman and XPS analysis

Since it is hard to complete identify CZTS phase based only on XRD results,[30,31] Raman spectroscopy was recorded on previous CZTS fibers for further identification as well as clarification of possible secondary phase. As can be seen from the Raman spectra shown in figure 5 that, a typical CZTS characteristic peak at about 337 cm^{-1} was observed, demonstrating CZTS phase formation in all three samples of CZTS-500, CZTS-550, CZTS-600.[32] Furthermore, A little uplift at around 286 and 363 cm^{-1} in the shoulder of peak 337 cm^{-1} in CZTS-550 and CZTS-600 further confirms the phase formation of CZTS compounds.[32]

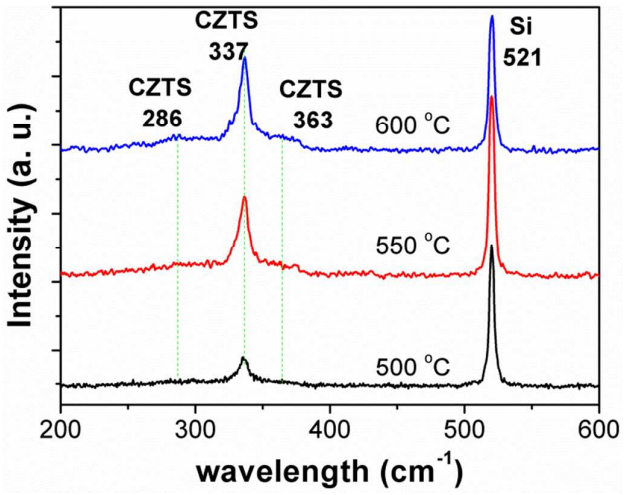

Fig. 5 Raman spectra of CZTS fibers obtained via vulcanization with varied temperature.

XPS characterization demonstrate very similar spectra, as shown in figure 6, for all vulcanized CZTS samples. A linear background subtraction is performed on the raw data, and the peaks are fitted using Gaussian method. As expected, all data from the spectra confirm the existence of Cu^{1+}, Zn^{2+}, Sn^{4+}, and S^{2-}, for the four elements in CZTS fibers, according to the previously reports[33,34] and XPS database. The

existence of Cu^{1+} is reasonably attributed by the two narrow peaks of Cu 2p at about 932.9 eV and 952.5 eV as shown in figure 6(a), Zn^{2+} is confirmed by Zn 2p located at 1022.5 eV and 1045 eV in figure 6(b), Sn^{4+} by Sn 3d at 486 eV and 494.8 eV, and S^{2-} in sulfide phase by S 2p located at 161.5 eV and 162.8 eV, respectively.[35]

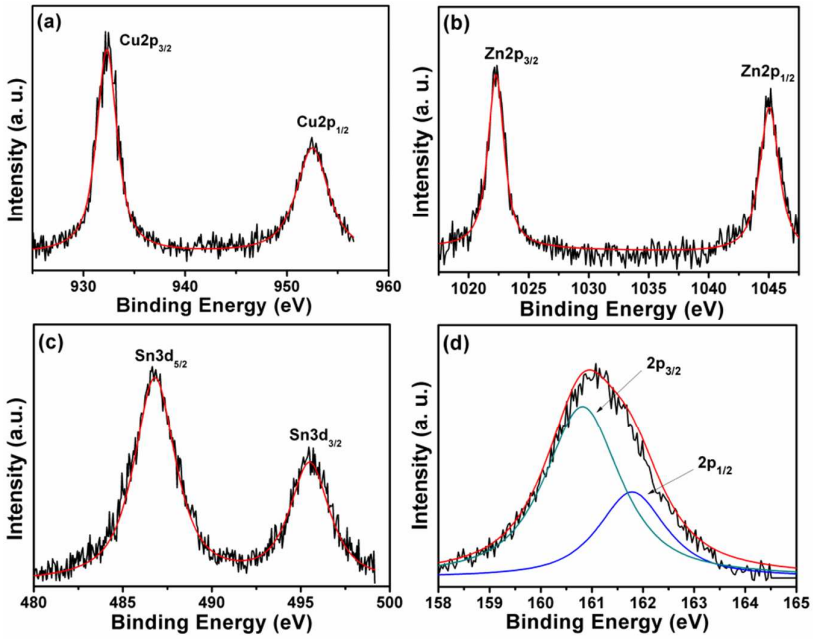

Fig. 6 XPS data for Cu, Zn, Sn and S elements in CZTS-550.

4.4 UV-vis absorption property

To estimate the band gap, the optical absorption property of CZTS fibers is investigated by UV-vis absorption spectroscopy using the reflection mode with integrating sphere accessory. In the reflection mode,

$$\frac{I_R}{I_0} = e^{-\alpha d} \quad (2)$$

where I_R is the reflecting optical intensity, I_0 is the original incident optical intensity, α is the absorption coefficient, and d is the film thickness. On the other hand, the absorbance value (Abs), which can be obtained directly via the spectrometer, is

defined as

$$Abs = \lg\frac{I_0}{I_R} \quad (3)$$

With the Combination of Eq.(2) and (3) we got

$$\alpha = \frac{ln10}{d} \cdot Abs \quad (4)$$

According to the famous *Tauc plot* method,[36][37] the optical band-gap E_g is estimated from the expression

$$(h\nu\alpha)^{1/n} = A(h\nu - E_g) \quad (5)$$

where h is Planck's constant, ν is the photon frequency, α is the absorption coefficient, and A is a proportionality constant. The value of the exponent n, which is the indication of the intrinsic radiative transition, equals to 1/2 in the case of semiconductors such as CZTS with direct optical transition. Thus the Eq.(5) follows

$$(h\nu\alpha)^2 = A(h\nu - E_g) \quad (6)$$

According to Eq.(6), E_g can be obtained from the slope of the linear fit of the $(h\nu\alpha)^2$- $h\nu$ curves. The curves and linear fit are depicted in figure 7, in which the film thickness d is about 100 μm obtained from its cross-section SEM image shown in the inset. As can be seen, E_g for all samples are at the value of about 1.5 eV, which is agreement with previously reports. More precisely, there is a little difference of E_g for CZTS samples annealed at varied temperatures, i.e., while E_g for CZTS-500 is almost the same of 1.48 eV, [26,33,38] it reduces to 1.43 eV for CZTS-550. E_g variation can generally be attributed to either secondary phase formation,[39] elemental substitution,[40] or crystal distortion.[41,42] The mechanism corresponding to E_g

reduction observed in orientational crystallized CZTS fibers may be related with strain or stress induced lattice distortion caused by crystal plane bending around the surface of CZTS micro or nano fibers, which needs further more detailed investigations. Nevertheless, E_g reduction would broaden the optical absorption spectrum thus increase the photoelectric efficiency of CZTS-based solar cell.

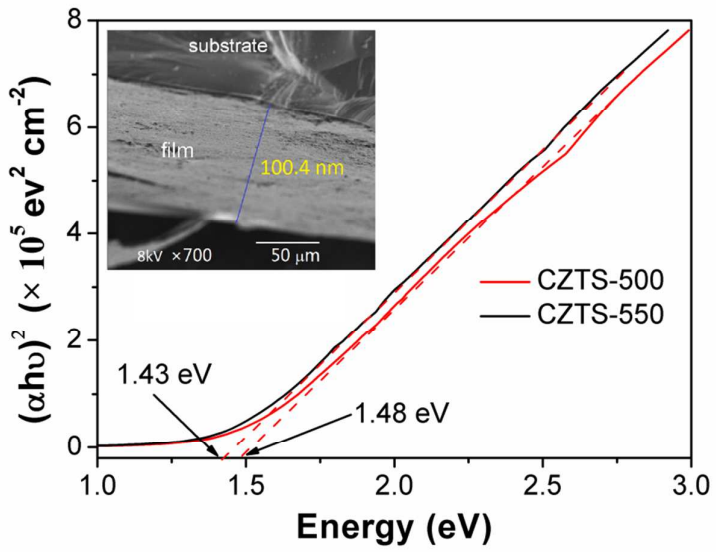

Fig. 7 Optical absorption effect of CZTS fibers obtained via vulcanization with varied temperature.

4. Conclusion

In this work, Cu_2ZnSnS_4 (CZTS) microfibers were fabricated using a non-vacuum method of electrospinning following vulcanization process. Low temperature vulcanization at 500 ℃ produced polycrystallized CZTS fibers with kesterite crystallization, while higher temperature vulcanization at and 550 ℃ led to a strong preferential crystallization along CZTS (112) crystal direction around fiber surface. Correspondingly, the band gap value E_g, which was 1.48 eV for CZTS-500, reduced to 1.43 eV for CZTS-550. Preferential crystallization as well as E_g reduction

shall be beneficial for exploring high-qualified CZTS using for CZTS-based solar cells with broadening optical absorption range and increased efficiency.

Acknowledgement

This work is financially supported by the National Natural Science Foundation of China with a grant number of 51402042 and 61106099, and the Fundamental Research Funds for the Central Universities of China ZYGX2013J117.

References

[1] P. Jackson, D. Hariskos, E. Lotter, S. Paetel, R. Wuerz, R. Menner, W. Wischmann and M. Powalla, *Prog. Photovolt: Res*. *Appl*., 2011, **19**, 894-897.

[2] R. Scheer, T. Walter, H. W. Schock, M. L. Fearheiley and H. J. Lewerenz, *Appl. Phys. Lett.*, 1993, **63**, 3294-3297.

[3] S. Ahmed, K. B. Reuter, O. Gunawan, L. Guo, L. T. Romankiw and H. Deligianni, *Adv. Ener. Mater.*, 2012, **2**, 253-259.

[4] I. Repins, M. A. Contreras, B. Egaas, C. DeHart, J. Scharf, C. L. Perkins, B. To, and R. Noufi, *Prog. Photovolt: Res*. *Appl*., 2008, **16**, 235-239.

[5] J. H. Shi, Z. Q. Li, D. W. Zhang, Q. Q. Liu, Z Sun and S. M. Huang, *Prog. Photovolt: Res*. *Appl*., 2011, **19**, 160-164.

[6] D. A. R. Barkhouse, O. Gunawan, T. Gokmen, T. K. Todorov, and D. B. Mitzi, *Prog. Photovolt: Res*. *Appl*., 2012, **20**, 6-11.

[7] K. Wang, O. Gunawan, T. Todorov, B. Shin, S. J. Chey, N. A. Bojarczuk, D. Mitzi, S. Guha, *Appl. Phys. Lett.*, 2010, **97**, 143508(1-3).

[8] Katagiri H, Jimbo K, Maw W S, O. Koichiro, Y. Makoto, A. Hideaki, T. Akiko, *Thin Solid Films*, 2009, **517**, 2455-2460.

[9] T. K. Todorov, J. Tang, S. Bag, O. Gunawan, T. F. Gokmen, Y. Zhu and D. B. Mitzi, *Adv. Mater.*, 2010, **22**, E156-E159.

[10] W. Wang, M. T. Winkler, O. Gunawan, T. F. Gokmen, Teodor K Todorov, Y. Zhu and D. B. Mitzi, *Adv. Energy Mater.*, 2014, **4**, 1301465.

[11] M. A. Green, K. Emery, Y. Hishikawa, W. Warta, E. D. Dunlop, *Prog. Photovolt.: Res. Appl.*, 2011, **19**, 565-672.

[12] I. Visoly-Fisher, S. Cohen, A. Ruzin, D. Cahen, *Adv. Mater.*, 2004, **16**, 879-883.

[13] C. S. Jiang, R. Noufi, K. Ramanathan, J. A. AbuShama, H. R. Moutinho, M. M. Al-Jassim, *Appl. Phys. Lett.*, 2004, **85**, 2625-2627.

[14] U. Rau, K. Taretto, *Appl. Phys. A*, 2009, **96**, 221-234.

[15] D. Azulay, O. Millo, I. Balberg, H. W. Schock, I. Visoly-Fisher, D. Cahen, *Solar Energy Materials and Solar Cells*, 2007, **91**, 85-90.

[16] W. K. Metzger, M. Gloeckler, *J. Appl. Phys.*, 2005, **98**, 063701.

[17] J. B. Li, V. Chawla, and B. M. Clemens, *Adv. Mater.*, 2012, **24**, 720-723.

[18] J. W. Li, D. B. Mitzi and V. B. Shenoy, *ACS Nano*, 2011, **5**, 8613-8619.

[19] L. Tsakalakos, J. Balch, J. Fronheiser, B. A. Korevaar1, O. Sulima and J. Rand, *Applied Physics Letters*, 2007, **91**, 233117(1-3).

[20] J. Wallentin, N. Anttu, D. Asoli, M. Huffman, I. Åberg, M. H. Magnusson, G. Siefer, P. Fuss-Kailuweit, F. Dimroth, B. Witzigmann, H. Q. Xu, L. Samuelson, K.

Deppert, M. T. Borgström, *Science*, 2013, **339**, 1057-1060.

[21] J. Tang, Z. Huo, S. Brittman, H. Gao, P. Yang, *Nat. Nanotechnol.*, 2011, **6**, 568-572.

[22] J. Xu, C. S. Lee, Y. B. Tang, X. Chen, Z. H. Chen, W. J. Zhang, S. T. Lee, W. X. Zhang, and Z. H. Yang, *ACS nano*, 2010, **4**, 1845-1850.

[23] L. Shi, C. Pei, Y. Xu, and Q. Li, *J. Am. Chem. Soc.*, 2011, **133**, 10328-10331.

[24] Z. Su, C. Yan, D. Tang, K. Sun, Z. Han, F. Liu, Y. Lai, J. Li, and Y. Liu, *CrystEngComm*, 2012, **14**, 782-785.

[25] C. P. Chan, H. Lam, K. K. Leung, C. Surya, *J. Nonlinear Opt. Phys. Mater.*, 2009, **18**, 599-603.

[26] K. C. Hsu, J. J. D. Liao, J. R. Yang, and Y. S. Fu, *CrystEngComm*, 2013, **15**, 4303-4308.

[27] Z. Q. Li, J. H. Shi, Q. Q. Liu, Y. W. Chen, Z. Sun, Z. Yang and S. M. Huang, *Nanotechnology*, 2011, **22**, 265615-265622.

[28] K. Oishi, G. Saito, K. Ebina, M. Nagahashi, K. Jimbo, W. S. Maw, H. Katagiri, M. Yamazaki, H. Araki, A. Takeuchi, *Thin Solid Films*, 2008, **517**, 1449-1452.

[29] T. Tanaka, D. Kawasaki, M. Nishio, Q. Guo, and H. Ogawa, *Phys. Stat. Sol. C*, 2006, **3**, 2844-2847.

[30] P. A. Fernandes, P. M. Salome and A. F. Da Cunha, *Thin Solid Films*, 2009, **517**, 2519-2523.

[31] X. Fontané, L. Calvo-Barrio, V. Izquierdo-Roca, E. Saucedo, A.

Pérez-Rodriguez, J. R. Morante, D. M. Berg, P. J. Dale and S. Siebentritt, *Appl. Phys. Lett.*, 2011, **98**, 181905(1-3).

[32] M. Himmrich and H. Haeuseler, *Spectrosc. Acta A*, 1991, **47**, 933-942.

[33] M. Cao, L. Li, B. L. Zhang, J. Huang, L. J. Wang, Y. Shen, Y. Sun, J. C. Jiang, G. J. Hu, *Solar Energy Materials&Solar Cells*, 2013, **117**, 81-86.

[34] Y. Liu, M. Ge, Y. Yue, Y. Sun, Y. Z. Wu, X. Chen, and N. Dai, *Phys. Status Solidi (RPL)-Rapid Research Letters*, 2011, **5**, 113-115.

[35] P. Dai, X. Shen, Z. Lin, Z. Feng, H. Xu and J. Zhan, *Chem.Comm.*, 2010, **46**, 5749-5751.

[36] J. Tauc, R. Grigorovici R and A. Vancu, *Phys. Status Solidi* b, 1966, **15,** 627-37.

[37] E. A. Davis and N. F. Mott, *Phil. Mag.*, 1970, **22**, 903-22.

[38] A. V. Moholkar, S. S. Shinde, A.R. Babar, K. U. Simb, Y. B. Kwonb, K. Y. Rajpurea, P. S. Patilc, C. H. Bhosalea, J. H. Kim, *Solar Energy*, 2011, **85**, 1354-1363.

[39] S. J. Ahn, S. Jung, J. Gwak, A. Cho, K. Shin, K. Yoon, D. Park, H. Cheong, and J. H. Yun, *Appl. Phys. Lett.*, 2010, **97**, 021905(1-3).

[40] Q. Guo, H. W. Hillhouse, and R. Agrawal, J. Am. Chem. Soc., 2009, **131**, 11672-11673.

[41] H. Wei, Z. Ye, M. Li, Y. Su, Z. Yang and Y. Zhang, *CrystEngComm*, 2011, **13**, 2222-2226.

[42] S. Chen, X. G. Gong, A. Walsh, and S. H. Wei, *Appl. Phys. Lett.*, 2009, **94**,

041903(1-3).